Engineering Fracture Mechanics 290 (2023) 109486

Contents lists available at ScienceDirect

Engineering Fracture Mechanics

journal homepage: www.elsevier.com/locate/engfracmech

Size correction scheme to determine fracture toughness with mini-CT geometry in the transition regime

Meng Li [a,b], Rachid Chaouadi [a], Inge Uytdenhouwen [a,*], Thomas Pardoen [b]

[a] Belgian Nuclear Research Centre (SCK CEN), Institute of Nuclear Materials Science (NMS), Boeretang 200, 2400 Mol, Belgium
[b] Institute of Mechanics, Materials and Civil Engineering (IMMC), Université catholique de Louvain, B-1348 Louvain-la-Neuve, Belgium

ARTICLE INFO

Keywords:
Fracture toughness
Ductile brittle transition
Local approach of fracture
Finite element modeling

ABSTRACT

The mini-CT geometry is used to determine relevant fracture toughness data along with the master curve description within the transition regime. However, due to significant loss of constraint experienced at loadings close to *J*-levels corresponding to the reference temperature T_0, the current size correction scheme from ASTM E1921 standard requires a better assessment in order to avoid censoring a large number of mini-CT specimens. Indeed, the current tight ASTM E1921 requirements on the K_{Jc} limit value set to ensure that the computed transition temperature T_0 is reliable often implies that many samples have to be censored. A large number of censored specimens leads to a significant loss of time, money and material, and of unnecessary activated material in the case of irradiated specimens. Besides, because of the specimen size reduction, more mini-CT samples and lower test temperatures as compared to large sized samples are required to determine a reliable T_0 value. In this study, an improved specimen size correction associated to the mini-CT geometry is proposed based on a local approach of brittle fracture combined with FEM simulations. The results show that the proposed size correction reduces the T_0 bias compared to the 1T-CT geometry. It also contributes to relaxing the K_{Jc} limit for the mini-CT geometry as compared to the ASTM size corrected values.

1. Introduction

Fracture toughness testing in the ductile-to-brittle transition range is essential for assessing the integrity of reactor pressure vessel (RPV) materials. After conducting measurements, the size adjustment of fracture toughness data leads to the evaluation of the transition temperature, T_0, and to the establishment of the master curve based on the ASTM E1921 standard [1]. This procedure plays a significant role in generating fracture toughness data over the ductile-to-brittle (DBT) region, in particular, in surveillance programs dealing with irradiation effects on RPV steels. A major issue in this context is the volume and spacing efficiency of the irradiated material due to the limited space inside the RPVs for irradiation. Therefore, the mini-CT geometry (Fig. 1), has attracted worldwide attention and studies as one of the most appealing miniaturized geometries [2–5]. Eight mini-CT specimens can be machined out of two broken halves, while machining with this cutting scheme makes the reorientation of the specimen possible. Another considerable advantage that enables this geometry to replace large ones is that former studies have demonstrated the validity of fracture toughness results extracted from mini-CT geometry [4,6–8].

However, as the specimen size is reduced, the crack-tip plastic zone developing from the free surfaces undergoes significant

* Corresponding author.
E-mail address: inge.uytdenhouwen@sckcen.be (I. Uytdenhouwen).

https://doi.org/10.1016/j.engfracmech.2023.109486
Received 31 December 2022; Received in revised form 5 July 2023; Accepted 10 July 2023
Available online 13 July 2023

expansion under increasing load. In turn, this strongly affects the size of the crack front over which high levels of near-tip stress triaxiality persist, when using stress triaxiality as an indicator of the level of constraint. The variation in the crack-tip stress fields over a relatively small thickness, combined with a smaller sampling volume for cleavage fracture, can influence the fracture toughness values, as well as their statistical scatter and mean value. Therefore, although the mini-CT geometry has been proven effective for the direct characterization of fracture toughness, a major drawback is that higher K_{Jc} value tends to be obtained because of significant loss of constraint at higher loading levels. Meanwhile, the reduction of specimen size leads to stricter K_{Jc} limit value. Although this limit value ensures that the computed transition temperature is close to the one produced by large CT specimens, it still comes at the cost of censoring a notable portion of test data. The censored K_{Jc} values will not be used for subsequent T_0 determination (only the number of censored K_{Jc} values is considered), thereby losing their ability to characterize fracture toughness, which will eventually lead to a serious loss of time and material, especially for irradiated materials.

The present study proposes and substantiates the validity of a modified size correction method based upon a local approach of fracture [9,10] framework incorporating the effects of plastic strain on brittle fracture. The objective is to provide a scheme which enables the characterization of the significant size effect associated to the mini-CT geometry, thereby producing a reliable transition temperature without censoring a lot of test data. In the first part of the paper, by relying on the Weibull stress, σ_w, as the local crack driving force, the parameters of the local approach are identified based on the test data from mini-CT geometry and finite element simulations of standard large CT geometries with a diverse range of constraints. Thereby, it ensures that the calibrated local approach is capable of correcting the measured toughness of mini-CT geometry to its 1T-size equivalent value. The second part of the paper explores the application of the proposed size correction method on the measured K_{Jc} values of mini-CT geometry in the transition regime, followed by the use of the size-adjusted K_{Jc} values to determine the transition temperature. In comparison to the existing size correction method in the ASTM standard, we will show this new size correction approach effectively adjusts the distribution of fracture toughness values of mini-CT geometry to a more reasonable level remarkably close to that of large CT geometries. The computed T_0 value is in better agreement with the corresponding estimates derived from large CT configurations even without applying the $K_{Jclimit}$, and it provides sufficient evidence for relaxing the $K_{Jclimit}$.

2. Consequences of using the mini-CT with current procedure

As specified in the ASTM E1921, before the calculation of T_0, the measured fracture toughness data are size-adjusted using the ASTM size correction:

$$K_{Jc(x)} = 20 + \left[K_{Jc(0)} - 20\right]\left(\frac{B_0}{B_x}\right)^{1/4}, \tag{1}$$

where $K_{Jc(x)}$ is the K_{Jc} for a specimen size B_x, $K_{Jc(0)}$ is the K_{Jc} for a specimen size B_0, B_0 is the thickness of the test specimens ignoring side grooves, B_x is the thickness of the specimens ignoring side grooves.

Then, censoring is made based on the validity limit of K_{Jc} value:

$$K_{Jclimit} = \sqrt{\frac{E(W - a_0)\sigma_{ys}}{30(1 - \nu^2)}}, \tag{2}$$

where E is the elastic modulus, W is the specimen width, a_0 is the pre-crack length, and ν is the Poisson ratio.

One of the drawbacks of ASTM E1921 is that the size correction scheme (see Eq. 1) employed in the Master Curve approach is based solely on the weakest link statistics [11–13]. It assumes that the fracture stress of a solid under stress depends only on the statistical distribution of microflaws uniformly distributed throughout its volume [10]. Thus, the geometries under consideration must exhibit the same scatter in their fracture toughness distributions. This implies that Eq. (1) can only be applied to the correction of geometries with high constraints that have comparable crack length-to-width ratios, but different thicknesses. The impact of constraint loss is not taken into account. Due to this limitation, Eq. (2) is not adapted to efficiently mitigate the significant loss of constraint that can be

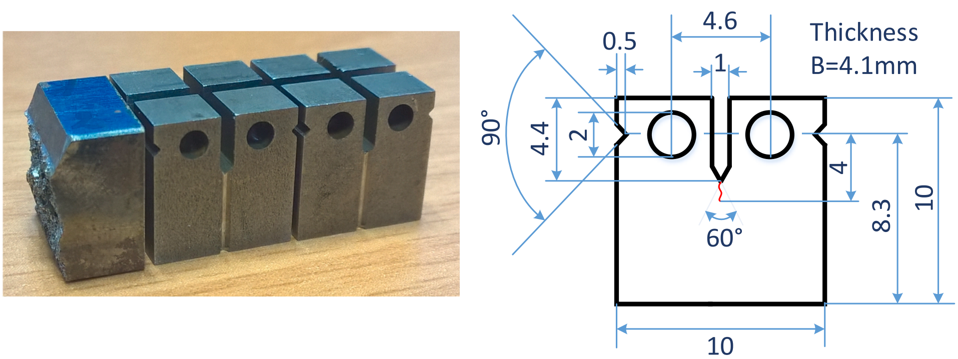

Fig. 1. Geometry of the mini-CT specimen.

observed with mini-CT specimens. As a result, the 1T-normalized K_{Jc} values obtained from the mini-CT specimens can be larger than the corresponding toughness levels extracted from large CT specimens tested at the same temperature if the mini-CT violates the ASTM E1921 size requirement. Larger 1T-normalized K_{Jc} value can potentially affect the evaluation of the transition temperature, T_0. Prior studies [4,14–20] have indicated that for certain RPV steels, the bias in the transition temperature between mini-CT geometry and large CT geometries can be over 10 °C. In addition, as indicated by Eq. (2), the reduction of specimen width leads to a lower $K_{Jclimit}$ value, which makes the mini-CT specimens with larger K_{Jc} values subject to stringent data censoring. This situation deteriorates for mini-CT specimens tested at higher temperatures.

The issues discussed above can be directly detected in actual experiments [4]. Fig. 2 displays the 1T-normalized K_{Jc} data of mini-CT, PCCv (pre-cracked Charpy v-notch), 4T-CT, 2T-CT, 1T-CT and 0.5T-CT specimens for the steel 22NiMoCr37. The test data for 4T-CT, 2T-CT, 1T-CT and 0.5T-CT specimens was obtained from the Euro fracture toughness dataset [4,21–23], which was generated in the framework of a European SM&T Project: “Fracture Toughness of Steel in the Ductile to Brittle Transition Regime”. The PCCv specimens were tested by three laboratories, NE, SCK CEN and VTT [21], the mini-CT specimens were tested at SCK CEN [4]. The Master Curve determined from the large CT geometries (0.5T-CT ~ 4T-CT) is added in the figure, the corresponding transition temperature, T_0, yields the value of -95 °C, note that only the data points in the relevant temperature range (-50 °C ≤ T_{test}-T_0 ≤ 50 °C) are plotted. The 1T-normalized K_{Jc} of mini-CT geometry has larger value compared to other geometries, and many of the data points are above the 95% confidence bound of the Master Curve (see for example Fig. 5 of PVP2016-63607). While it is true that most of the data above 95% confidence bound needs to be censored and they do not significantly affect T_0 estimation, this observation highlights a limitation of the current size correction method that it is unable to reduce the K_{Jc} of mini-CT specimens to the same level as large CT specimens. Significant difference on $K_{Jclimit}$ value is also observed, where smaller geometries have lower $K_{Jclimit}$. At -120 °C and -115 °C, about half of the data points of mini-CT geometry are above the $K_{Jclimit}$, which means they have to be censored. For the PCCv geometry and 0.5T-CT geometry, similar situations are observed at -90 °C and -60 °C, respectively, they are less affected by their $K_{Jclimit}$. In particular, the 1T-CT geometry does not have this problem, the $K_{Jclimit}$ of 1T-CT geometry falls on the 95% confidence bound at the upper bound of the test temperature allowance (~-50 °C), which will hardly cause any waste of test data. The summary of the data censoring of these geometries is listed in Table 1; it is observed that although the test temperature range of $T_0 \pm 50$ °C has been strictly restricted because the load-carrying capacity of small size specimens does not allow testing at high temperatures due to enhanced loss of constraint [4], there are still 23.5% of the mini-CT data points exceeding the $K_{Jclimit}$, which means that a large proportion of test data are censored. In contrast, for large CTs such as 0.5T-CT, 1T-CT, 2T-CT and 4T-CT, few or even no test data are censored. Note that for the PCCv geometry, the high percentage of censored data is due to the fact that the tests were conducted over a wide temperature range, resulting in a significant portion of the test data at higher temperature exceeding the measuring capacity. In addition, in the context of the T_0 evaluation, although the presence of data censoring procedure ensures the acceptability of T_0, Table 1 demonstrates that the calculated T_0 of the mini-CT geometry is still affected by the potential effect of constraint loss. Specifically, the T_0 value of the mini-CT geometry is more than 10 °C lower compared to the T_0 values extracted from large geometries, as indicated in Table 1.

Moreover, Fig. 3 assesses the effectiveness of the ASTM size correction equation, irrespective of the data censoring procedure. The 1T-normalized fracture toughness of all the CT specimens are converted into the corresponding estimated toughness at -115 °C assuming that each specimen follows its own master curve. It is clear that the large CT geometries (0.5T-CT ~ 4T-CT) show relatively close toughness distributions, the scatter of the 1T-normalized K_{Jc} of large CT specimens yields 71 ± 19 MPa$\sqrt{m}$. However, the size corrected toughness of mini-CT geometry is broadly overestimated. The scatter of the 1T-normalized K_{Jc} yields 94 ± 31 MPa$\sqrt{m}$, which exceeds the upper bound of the 1T-normalized K_{Jc} defined by large CT geometries. Above all, it is clear that the existing size correction approach cannot effectively normalize the K_{Jc} of mini-CT to a reasonable range which is similar to that of large CT

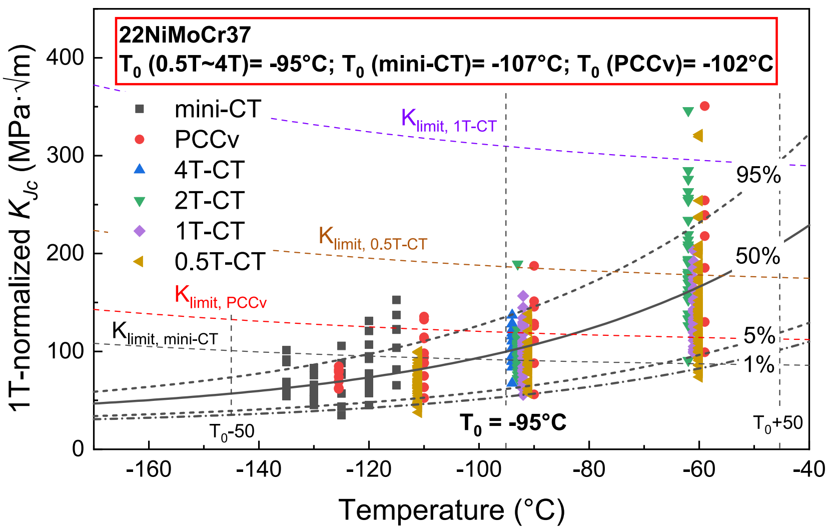

Fig. 2. Fracture toughness distribution of 22NiMoCr37 in the temperature range of interest [4,21–23].

Table 1
Summary of the data censoring.

	Mini-CT	PCCv	0.5T-CT	1T-CT	2T-CT	4T-CT
T_{test} range, °C	[-135,-115]	[-125,-60]	[-110,-60]	[-90,-60]	[-90,-60]	[-90]
N	51	44	180	107	92	15
r	39	29	169	107	92	15
Percentage of censored data $(N\text{-}r)/N$	23.5%	34.1%	6.1%	0	0	0
T_0, °C	-107	-102	-87	-91	-97	-90

N = the total number of test data, r = the number of the uncensored data.

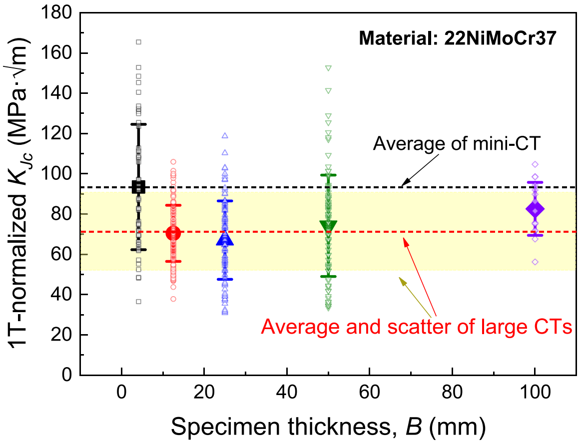

Fig. 3. The 1T-normalized K_{Jc} distributions of CT geometries at -115 °C.

geometries. And with the strict limit on K_{Jc} value, many test data are censored and replaced, which eventually leads to a serious waste of test resources. Therefore, a better size correction approach specifically designed for the mini-CT geometry is required, based on which the relaxation of the $K_{Jclimit}$ can be discussed.

3. Finite element procedures and local approach to brittle fracture

3.1. Material properties

The material is the typical reactor pressure vessel (RPV) steel 22NiMoCr37. The chemical composition is given in Table 2. The present study mainly focuses on the fracture toughness of CT specimens in the ductile-to-brittle transition (DBT) regime, hence the mechanical properties of 22NiMoCr37 were generated from tests on mini round tensile bars with 15 mm gauge length and 3 mm diameter at a temperature close to the transition temperature, which is T_{test} = -110 °C. Bridgman's stress correction [24] was then applied to give an approximation of the true stress at fracture. The true stress–strain curve of 22NiMoCr37 at -110 °C is given in Fig. 4, the corresponding mechanical properties are given in Table 3.

3.2. Finite element modeling

Finite element simulations were performed using the commercial package ANSYS. Fig. 5 shows the finite element models of (a) mini-CT specimen and (b) standard large CT specimen. The J_2 flow theory was assumed using the following hardening law

$$\sigma = \sigma_{ys}\left(1 + \frac{E\varepsilon^{pl}}{\sigma_{ys}}\right)^n, \tag{3}$$

where n is the strain-hardening exponent.

The geometry of the mini-CT specimen is identical to the real experimental specimen, with dimensions given in Table 4. As shown in Fig. 5, the mini-CT specimen was analyzed using one-half of the 3-D model with a symmetric boundary condition imposed on the

Table 2
Chemical composition (weight%).

Material	C	Si	Mn	S	P	Cr	Ni	Mo	Cu
22NiMoCr37	0.22	0.23	0.88	0.004	0.006	0.39	0.84	0.51	0.08

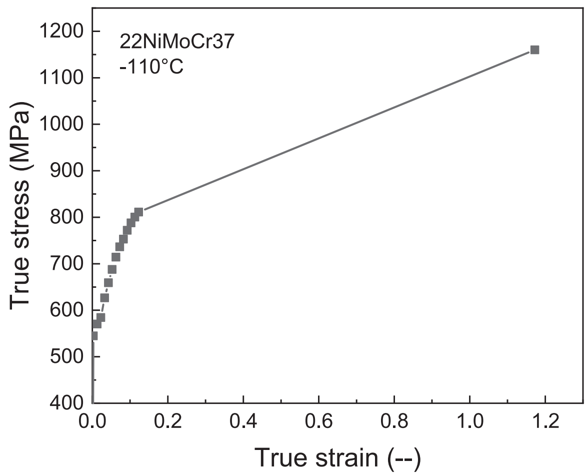

Fig. 4. Experimental true stress-true strain curve for 22NiMoCr37 steel at -110°C.

Table 3
Mechanical properties extracted from uniaxial tensile test.

Material	T (°C)	E (GPa)	ν	σ_{ys} (MPa)	ε_{uts}	σ_{uts} (MPa)	$\sigma_{F,Bridgman}$(MPa)
22NiMoCr37	-110	213.6	0.3	577	0.139	719	1160

T = test temperature, E = Young's modulus, ν = Poisson's ratio, σ_{ys} = yield strength, ε_{uts} = strain at uts, σ_{uts} = ultimate tensile strength.

remaining ligament plane. The finite element model was 20% side grooved and loaded by applying displacement on the pin model. Contact elements were applied between the pin and the specimen to simulate the interaction. The meshing was highly refined in the mean crack tip region, a "spider web" [25] mesh configuration with concentric rings of quadrilateral elements was built to accurately evaluate the local J-integral along the pre-crack front. The fatigue pre-crack was modeled as an initial notch with finite radius. Prior research suggested that an initial crack-tip notch radius more than 5 times lower than the CTOD at crack initiation minimizes the effect of initial crack-tip notch on the stress and strain fields near the crack tip [10,26–28]. In addition, it was found in the subsequent investigations on the effect of crack-tip notch that close Weibull stress can be obtained from the pre-crack configurations with $\rho_0 =$ 0.005 mm and $\rho_0 = 0.01$ mm. Much of the difference that is potentially observed can be compensated by sufficient mesh refinement. It indicates a limited effect of crack-tip notch radius on the computed results. An extremely small notch radius (e.g. $\rho_0 = 0.0025$ mm) is also undesirable because it leads to unexpected extensive element distortion at the near tip region [27,29]. Consequently, a notch radius $\rho_0 = 0.005$ mm is considered in this study to provide accurate simulations of sharp crack front and stable numerical convergence.

The 3-D finite element simulations are conducted on the plane-sided standard large CT geometries (0.5TCT, 1T-CT and 2T-CT). The dimensions of the standard large CT specimens are listed in Table 4. The finite element models of large CT specimens have a similar crack front configuration and mesh arrangement as described for the mini-CT specimen model. As shown in Fig. 5, the simulation of the one-quarter 3-D finite element model was made possible owing to the symmetry conditions. Symmetry boundaries were imposed on the remaining ligament plane ($Y = 0$) and the mid-thickness plane ($X = 0$). The variation of the stress- strain distribution over the thickness of the large CT specimen requires variable mesh layers to increase the simulation accuracy, the defined mesh layer thickness increases from the thickest division at the symmetric plane ($X = 0$) to the thinnest division at the free surface ($X = B/2$) [27]. Similarly, the displacement was applied to the pin to simulate the real loading process.

Table 4
Dimensions of the specimens.

Geometries	Dimensions			
	W (mm)	B (mm)	a_0/W	Side-grooving
Mini-CT	8.3	4.1	0.5	20%
0.5T-CT	25	12.5	0.55	0
1T-CT	50	25	0.55	0
2T-CT	100	50	0.55	0

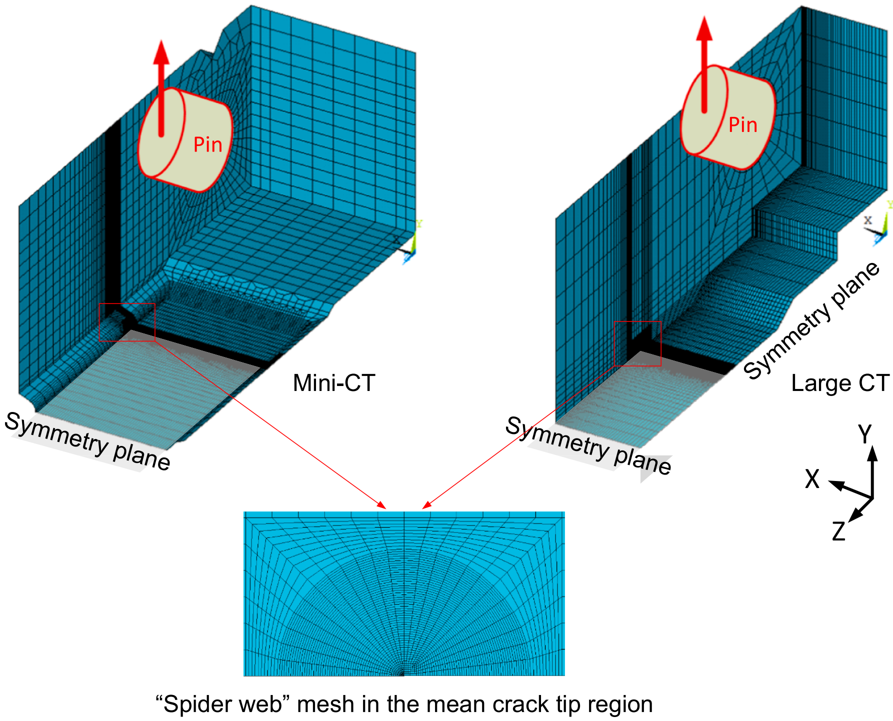

Fig. 5. Finite element model of mini-CT specimen and large CT specimen.

3.3. Basic principles of the local approach to brittle fracture

The development of probabilistic models for cleavage fracture has always played an important role in fracture mechanics. The Beremin group [30,31] proposed principles of micromechanics-based modeling of brittle fracture, and has served over the past few decades as the basis for the determination of the fracture toughness relying on different geometries and loading modes. The core principle is that the size of the micro-cracks in the material is distributed according to simple statistical laws, such as a power law or an exponential law. Following the weakest link hypothesis, it is assumed that brittle fracture is triggered when the most severe Griffith-like micro-crack runs unstably in the stressed region. The probability of finding such a micro-crack is related to the volume of material undergoing plastic deformations. The Beremin model introduced the Weibull stress, σ_w, to describe such a local condition leading to failure, which can be expressed as

$$\sigma_w = \left(\int_{PZ} \frac{\sigma_1^m dV}{V_0} \right)^{\frac{1}{m}} = \sigma_u \left(\ln \left[\frac{1}{1 - P_R} \right] \right)^{\frac{1}{m}}, \tag{4}$$

where m is the Weibull shape parameter, σ_1 is the maximum principal stress, V_0 is the representative volume element, dV is the incremental volume over the plastic zone (PZ), P_R is the probability of failure, σ_u is the Weibull scale parameter. In the original formulation, m and σ_u are material constants, which are temperature independent.

The main drawback of the original Beremin model is that it ignored the potential effect of plastic strain on the microscopic process of brittle fracture, leading to inaccurate estimate of the failure probability. Based on arguments by Wallin et al. [32] that only a portion of all fractured particles eventually contributes to the brittle fracture process, an approach incorporating the effects of plastic strain through the particle fracture stress was proposed, namely the particle distribution model [10]. The Weibull stress in this model is expressed as

$$\sigma_w = \left[\frac{1}{V_0} \int_{\Omega} \left\{ 1 - \exp \left[- \left(\frac{\sigma_{pf}}{\sigma_{prs}} \right)^{\alpha_p} \right] \right\} \sigma_1^m d\Omega \right]^{\frac{1}{m}}, \tag{5}$$

where Ω is the volume of the near tip fracture process zone which is defined as the region where $\sigma_1 \geq \psi \sigma_{ys}$, with σ_{ys} indicating the material yield strength and ψ most often being equal to 2, σ_{prs} is the particle reference stress, which represents an approximate average of the distribution of particle fracture stress in the given material, α_p is the Weibull modulus, which generally takes the value of 4 for ferritic structural steels, σ_{pf} is the particle fracture stress, $\sigma_{pf} = \sqrt{1.3\sigma_1 \epsilon_p E_d}$, in which ϵ_p is the effective matrix plastic strain and E_d is the elastic modulus of the particle, with $E_d = 400$ GPa for ferritic steels.

The two parameters that play an important role in the local approach (particle distribution model), i.e. the Weilbull shape parameter, m, and the particle reference stress, σ_{prs}, need to be calibrated for the later calculation of σ_w. The m factor characterizes the shape of the Weibull stress distribution, as indicated above, it is also a weight factor to the stresses in the near tip region. σ_{prs} has a direct bearing on the impact of the plastic strain, for a certain deformation level, the increase of σ_{prs} indicates an increasing effect of plastic strain. It should be noted that we selected a 2-parameter rather that 3-parameter Weibull distribution model [33,34] in order to reduce the number of parameters to identify. Moreover, the objective of the model is not to predict fracture toughness but mainly to access to local damage parameters for comparison between the mini-CT and the 1T-CT specimens.

3.4. Identification of the local approach parameters

The procedure follows a two-step strategy to determine the m factor and σ_{prs}. As shown in Fig. 6, the present framework first starts

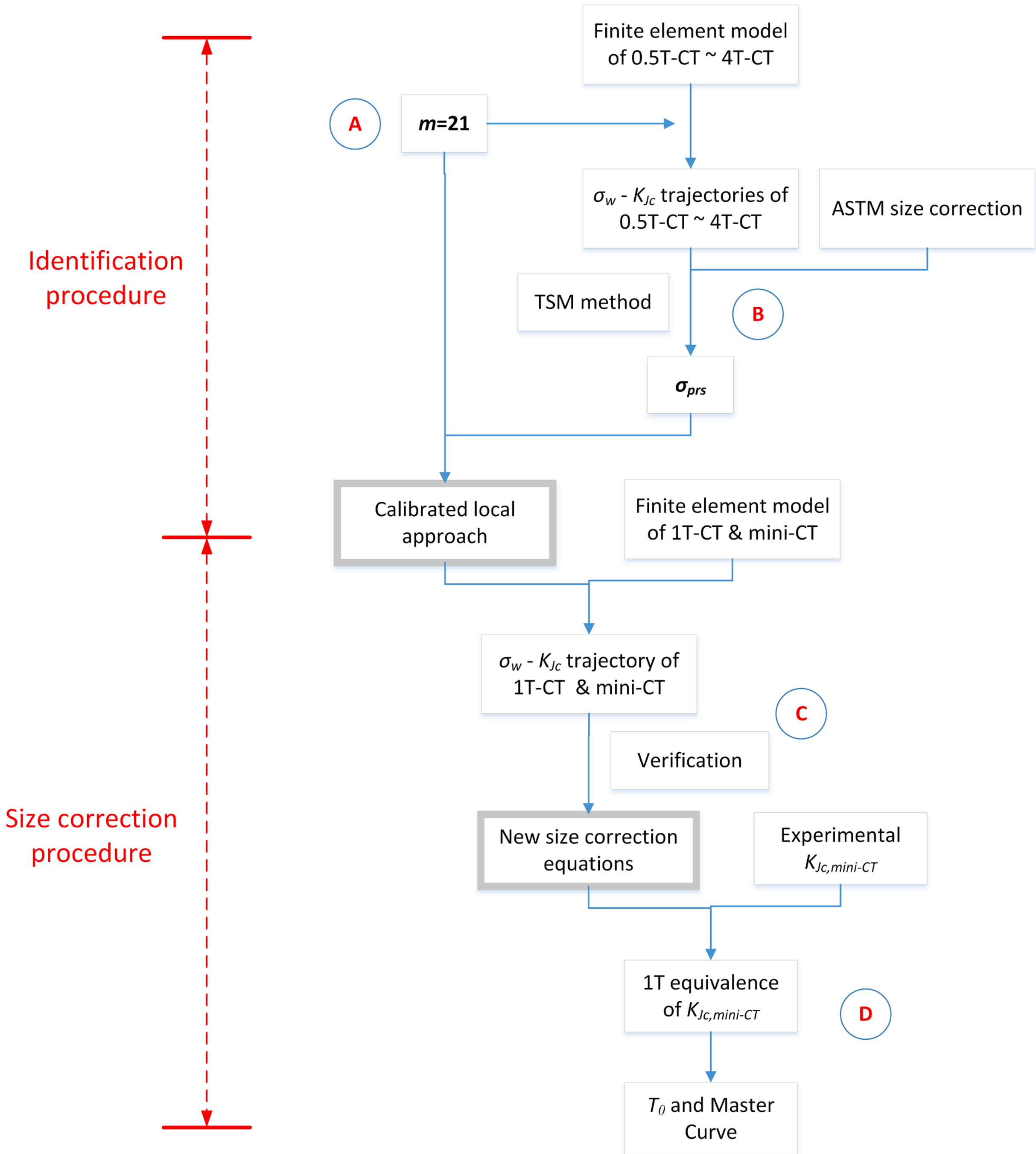

Fig. 6. Schematic of the proposal of the new size correction method.

by selecting the m factor based on literature for the material under investigation or alternatively linear fitting of experimental data that are essentially under SSY conditions over an extended test temperature range (Step A). Then the σ_w - 1T-normalized K_{Jc} trajectories of 0.5T-CT, 1T-CT, 2T-CT and 4T-CT are computed using the nonlinear finite element analysis based on the calibrated Weibull factor, m. Finally, a σ_{prs} is identified in such a way that it enables the local approach to accurately describe the performance of the size correction method [1] among large CT geometries (Step B).

The size correction procedure starts with the verification of the accuracy of the calibrated local approach (Step C). Once good verification results are obtained, the new size correction equations are generated based on the σ_w - K_{Jc} trajectories of 1T-CT and mini-CT that are computed using the local approach. Finally, the proposed new size correction equations are adopted on the experimental K_{Jc} of mini-CT to compute the reference temperature, T_0 and to evaluate the Master Curve (Step D).

Firstly, in the analysis to be discussed, the m factor is selected to be equal to 21, which compares well to previously reported m-values for RPV steels exhibiting similar hardening behavior [11,30,35–43]. In addition, in this work, an identification method proposed by Andrieu [35] is adopted to support the selected value of m factor based on available experimental data. The details of the identification procedure are as follows. Early contributions by Beremin group [30] showed that the Beremin expression under small

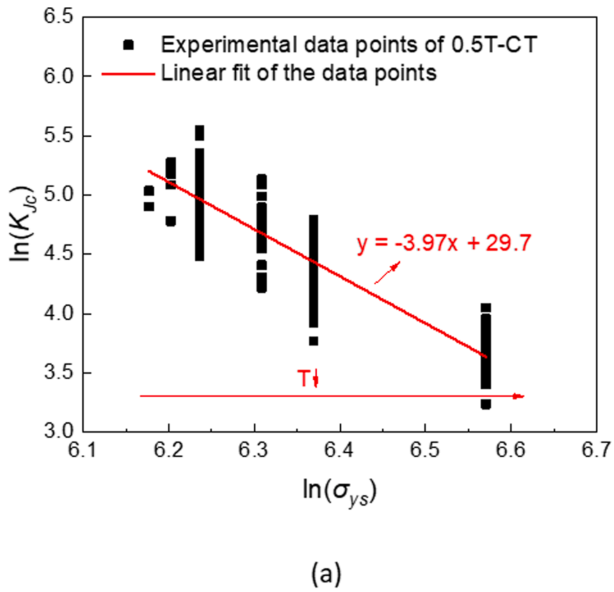

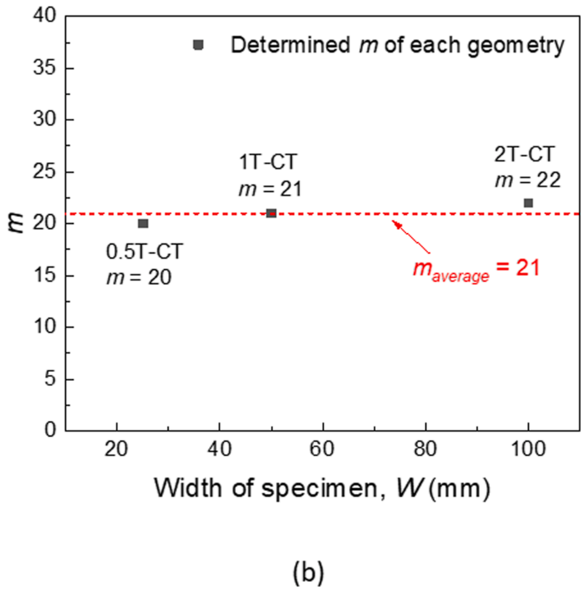

Fig. 7. (a) Experimental $\ln(K_{Jc})$ - $\ln(\sigma_{ys})$ data and their linear fitting (b) Determination of m based on all CT geometries.

scale yielding (SSY) and plane strain conditions can be written as

$$\ln\left(\frac{1}{1-P_r}\right) = \frac{BK_{Jc}^4\sigma_{ys}^{m-4}C_{m,n}}{V_0}, \tag{6}$$

where B is the specimen thickness; K_{Jc} is the measured fracture toughness; σ_{ys} is the yield strength; C_{mn} is a function of m and n but independent on K_{Jc}, σ_{ys} and E; V_0 is the representative element volume. For a given failure probability, $K_{Jc}^4\sigma_{ys}^{m-4}$ is a constant value, written as $K_{Jc}^4\sigma_{ys}^{m-4} \equiv b$. Applying the logarithm on both sides of the equation, the equation can be expressed as

$$\ln(K_{Jc}) = -\frac{m-4}{4}\ln(\sigma_{ys}) + \frac{\ln b}{4}. \tag{7}$$

The identification methodology developed by Andrieu [35] suggested to plot the variation of the experimentally measured $\ln(K_{Jc})$ with $\ln(\sigma_{ys})$ in order to determine m through linear fitting. The slope of the linear fitting, a, can be expressed as a function of m factor:

$$a = -\frac{m-4}{4}. \tag{8}$$

In Fig. 7(a), an example of determination of the m factor using the method outlined above is presented for the case of 0.5T-CT specimens tested in a temperature range between -154 °C and -20 °C and that are not exceeding the $K_{Jclimit}$. First, a linear regression is applied to the experimental data pairs ($\ln(K_{Jc})$ - $\ln(\sigma_{ys})$) obtained from the 0.5T-CT specimens tested at various temperatures. Based on the slope of the linear regression, the m factor is calculated using Eq. (8), after rounding to the closest integer, giving $m = 21$. In order to identify a robust m factor for studying mini-CT specimens made of 22NiMoCr37 material, the same procedure was followed for the experimental data on the geometries exhibiting SSY-conditions over a large test temperature range and with an adequate number of tests (0.5T-CT, 1T-CT and 2T-CT). The results are presented in Fig. 7(b). The average m factor value for these geometries is found to be equal to 21, which closely aligns with the value selected above. According to the research on the Euro-material conducted by Wasiluk [42], the m factor, as a phenomenological description of Griffith-like micro-cracks that lead to brittle fracture, is independent of test temperature in the 22NiMoCr37 RPV steel. Therefore, the m factor is considered to have a fixed value for the material 22NiMoCr37 in the following analysis. Note that another value of the m factor falling within the acceptable range for this class of materials would lead to equally acceptable results because of the degree of freedom in the identification of the second parameter to which it is related (σ_{prs}). It is worth mentioning that the identification procedure of the m factor provided by Andrieu is solely aimed at providing support for the selection of m value. This procedure, utilized in the current study, enables the generation of meaningful results for the analyzed RPV steels, such as 22NiMoCr37 and 73W. Nevertheless, conducting additional verification studies is crucial to establish the validity of this method across a wider range of steels and conditions.

The identification of σ_{prs} requires the toughness scaling model (TSM) proposed by Ruggieri and Dodds [44] which relies on the Weibull stress approach to take into account the constraint effects on the fracture toughness. As addressed above, the Weibull stress is derived from the crack tip local condition and can be interpreted as the driving force of the brittle fracture. As shown in Fig. 8, for the same material and test condition, a specific critical Weibull stress ($\sigma_{w,critical}$) needs to be attained to trigger cleavage for the geometries with different constraints (geometry A and B), although deviations in the K_{Jc} values ($K_{Jc\text{-}A}$ and $K_{Jc\text{-}B}$) can be expected due to constraint loss. For standard large CT geometries, the ASTM E1921 provides a size correction methodology (Eq. (1)) that enables the conversion of the fracture toughness value between them. Indicating that for different large CT geometries, the K_{Jc} values corresponding to a certain critical Weibull stress can come to a good agreement after the ASTM size correction, that is, the σ_w - K_{Jc} curves overlap with one another. Therefore, a σ_{prs} is found to provide the best curve-overlap between large CT geometries after the size correction of K_{Jc} value.

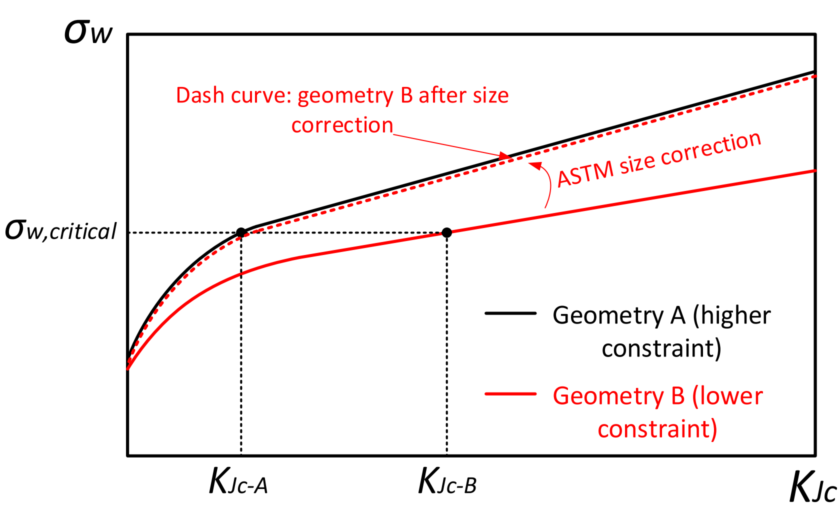

Fig. 8. Schematic of the procedure to transpose fracture toughness from one geometry to another (toughness scaling model).

With the maximum measured fracture toughness ratio of $K_{Jc,0.5T\text{-}CT}/K_{Jc,4T\text{-}CT} \sim 1.68$, the sufficient large constraint difference between 0.5T-CT, 1T-CT, 2T-CT and 4T-CT ensures that an accurate calibrated σ_{prs} can be provided. Therefore, these four geometries are used in the following identification procedure where the TSM method is involved.

Fig. 9(a-c) provide the variation of the Weibull stress with the FEM computed K_{Jc} value. The Weibull stress is normalized by the yield strength of 22NiMoCr37 at -110 °C, the K_{Jc} value is converted to the 1T size equivalence based on the size correction formulae proposed by the ASTM E1921. These plots clearly show the effect of σ_{prs} on the Weibull stress curves for the different specimen sizes. When $\sigma_{prs} = 2000$ MPa, 4T-CT geometry has the largest normalized Weibull stress, in particular at larger K_{Jc} value. As σ_{prs} increases, the curves derived from the 1T-CT, 2T-CT and 4T-CT FEM models always show close agreement, the Weibull stress calculated from the 0.5T-CT model gradually increases compared to the other two geometries. The normalized Weibull stress of mini-CT varies differently with increasing load, which makes it difficult for the curve of mini-CT to overlap with other geometries. Therefore, in these plots, only when $\sigma_{prs} \sim 5000$ MPa is the ASTM size correction such that the Weibull stress curves of large CT geometries agree with one another. The results displayed above show that the largest difference between the Weibull stress curves is mainly found between the geometries with the largest constraint difference: 0.5T-CT and 4T-CT. In order to determine a relevant value for σ_{prs} that will be used next, Fig. 9(d) plots the 1T-normalized K_{Jc} correlations between the 0.5T-CT and 4T-CT geometries. Each curve provides pairs of K_{Jc} values in the 0.5T-CT and 4T-CT geometries which produce the same normalized Weibull stress, illustrating the same probability of triggering brittle fracture. All normalizations of the K_{Jc} values are based on the standard ASTM E1820. A curve defining $K_{Jc,0.5T\text{-}CT} = K_{Jc,4T\text{-}CT}$ is included in the plot to provide a reference. The K_{Jc} correlation is clearly affected by the σ_{prs}, and this dependence is weakened at larger σ_{prs}. Here, an increase of σ_{prs} results in a larger ratio of $K_{Jc,4T\text{-}CT}$ and $K_{Jc,0.5T\text{-}CT}$. $K_{Jc,4T\text{-}CT}$ and $K_{Jc,0.5T\text{-}CT}$ shows the closest agreement when σ_{prs} is between 4000 MPa and 5000 MPa. Finally, by finding the best correction for the computed K_{Jc} at -110 °C for 0.5T-CT and 4T-CT, σ_{prs} is identified to be equal to 3800 MPa.

The σ_w - size corrected K_{Jc} trajectories computed using the calibrated parameters are shown in Fig. 10, the σ_w - size corrected K_{Jc} trajectory of mini-CT geometry is also added for reference. Remarkably close agreement between the curves corresponding to the large CT geometries is found, whereas the mini-CT geometry still shows deviation due to constraint loss.

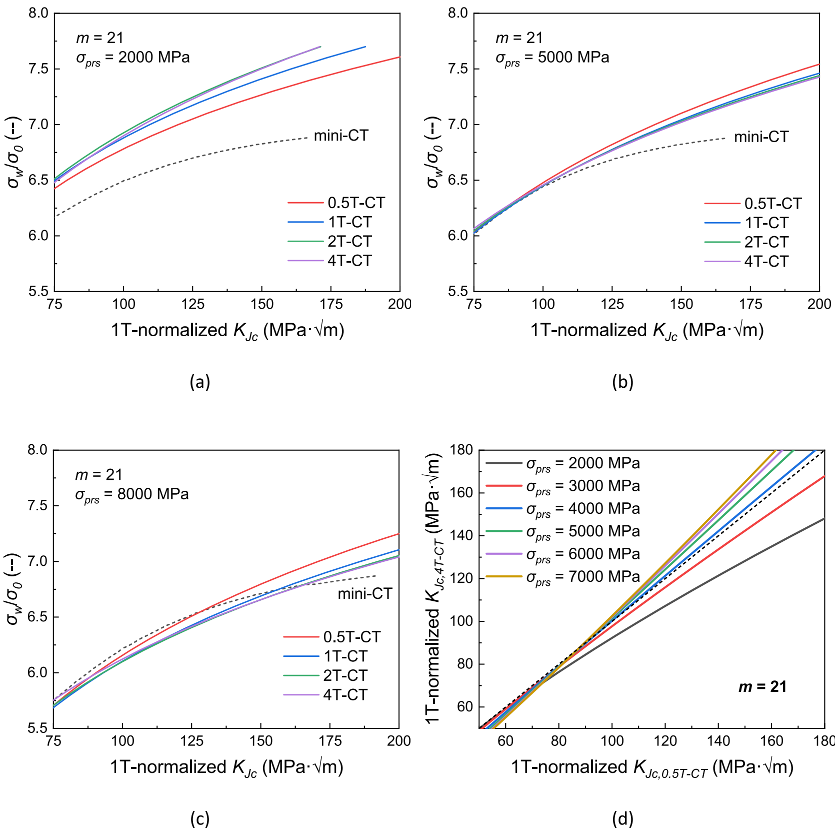

Fig. 9. Variation of σ_w/σ_0 as a function of 1T-normalized K_{Jc} with (a) $\sigma_{prs} = 2000$ MPa (b) $\sigma_{prs} = 5000$ MPa (c) $\sigma_{prs} = 8000$ MPa (d) Constraint correlations of 1T-normalized K_{Jc} values of 0.5T-CT and 4T-CT geometry.

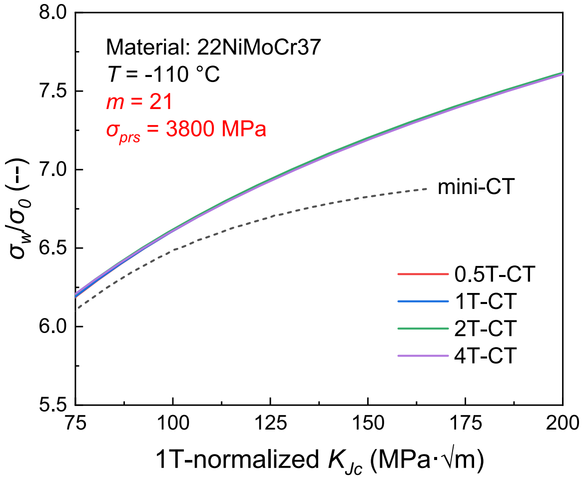

Fig. 10. Evolution of σ_w/σ_0 with increasing 1T-normalized K_{Jc} with $m = 17$ and $\sigma_{prs} = 4200$ MPa.

4. Size correction of the fracture toughness in the transition regime

4.1. New size correction scheme

To verify the predictive capability of the local approach as identified before, the Weibull stress based approach is applied to correct the fracture toughness value of mini-CT geometry to the 1T-normalized equivalence. The Weibull fitting parameter, K_0, characterizes the fracture toughness value corresponding to the 63.2% cumulative failure probability level (ASTM E1921). It is considered as a characteristic value of different geometries in the toughness scaling model. Previously, a large number of fracture toughness tests have been performed in the transition regime inside and outside SCK CEN to determine the reference temperature, T_0, for the 22NiMoCr37 RPV steel. The evaluation procedure of T_0 is carried out separately for mini-CT and other standard large CT geometries. Following the evaluation procedure in ASTM E1921, for standard large CT geometries (0.5T-CT ~ 4T-CT), the reference temperature is equal to -95 °C. For the mini-CT geometry, the reference temperature is equal to -107 °C, which is 12 °C below large CT specimens. The Weibull fitting parameter, K_0, of large CTs and mini-CT can thus be calculated based on the T_0 determined previously using

$$K_{Jc(med)} = 30 + 70exp[0.019(T - T_0)], \tag{9}$$

$$K_0 = 20 + \left(\frac{1}{0.91}\right)\left(K_{Jc(med)} - 20\right), \tag{10}$$

where T is the test temperature, T_0 is the reference temperature, and $K_{Jc(med)}$ is the median toughness. Eq. (9) is known as the final form of the Transition Temperature Curve (Master Curve), it gives the dependence of the median fracture toughness as a function of test temperature. The estimated K_0 are listed in Table 5.

Fig. 11(a) displays the computed σ_w - K_{Jc} curves based on the local approach with the calibrated parameters: $m = 21$, $\sigma_{prs} = 3800$ MPa, for mini-CT geometry and 1T-CT geometry at -110 °C. The Weibull stress, σ_w, is normalized by the material yield strength, σ_0 (refer to Table 3), the K_{Jc} is the fracture toughness value determined based on the load-CMOD curve derived from the finite element simulations. As outlined in the previous section, the toughness scaling methodology (TSM) assumes that cleavage is triggered when a certain Weibull stress is attained for different geometries. Therefore the 1T size equivalence of $K_{0,mini\text{-}CT}$ is determined to be the K_{Jc} of 1T-CT geometry that corresponds to the critical Weibull stress defined by $K_{0,mini\text{-}CT}$. Then the Weibull scale parameter corresponding to the 1T-CT geometry, $K_{0,1T\text{-}CT}$, is determined to be equal to 94.1 MPa$\sqrt{\text{m}}$. This value must be compared to the experimental $K_{0,1T\text{-}CT}$ equal to 88.8 MPa$\sqrt{\text{m}}$, with thus only 5.3 MPa$\sqrt{\text{m}}$ difference. In the next step, based on the σ_w - K_{Jc} trajectories of 1T-CT geometry and mini-CT geometry plotted in Fig. 11(a), the correlations between the fracture toughness of the mini-CT geometry, $K_{Jc,mini\text{-}CT}$, and its 1T size equivalence is given in Fig. 11(b). For reference, the 1T-normalized $K_{Jc,mini\text{-}CT}$ value obtained using the ASTM size correction method is also indicated, which holds a linear relationship with the increased loading. In the early loading stage, typically when K_{Jc},

Table 5
The size corrected K_0 at -115 °C.

Specimen	T (°C)	Experimental results		Local approach predictions
		T_0 (°C)	K_0 (MPa$\sqrt{\text{m}}$)	K_0 (MPa$\sqrt{\text{m}}$)
Mini-CT	-115	-107	151.4	151.4
1T-CT	-115	-95	88.8	94.1

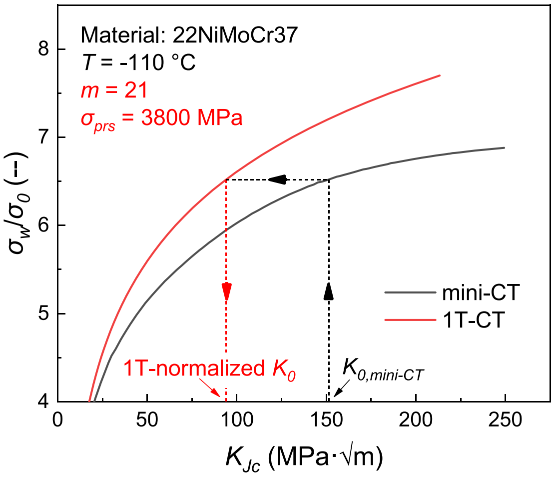

(a)

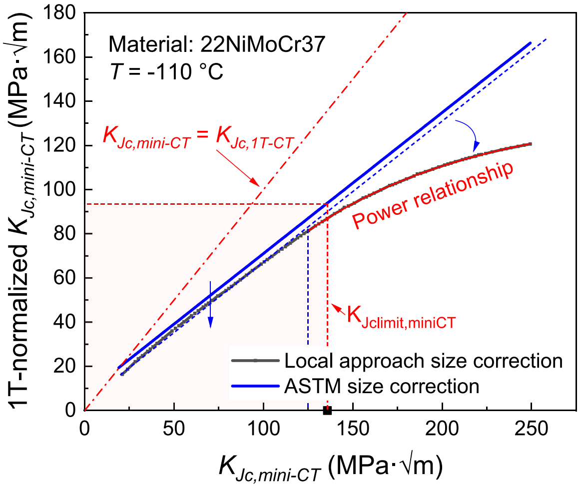

(b)

Fig. 11. (a) Variation of σ_w/σ_0 as a function of K_{Jc} for 1T-CT geometry and mini-CT geometry, (b) Correlations of 1T-normalized K_{Jc} and the K_{Jc} measured from mini-CT specimen.

$_{mini\text{-}CT} < 125$ MPa$\sqrt{}$m, the ASTM size correction can provide relatively close results with the predicted results using the local approach. When $K_{Jc,mini\text{-}CT} \geq 125$ MPa$\sqrt{}$m, the correlation $K_{Jc,mini\text{-}CT} \rightarrow$ 1T-normalized $K_{Jc,mini\text{-}CT}$ leads to a power law relationship. The ASTM size correction shows a relatively poor performance, thus confirming that the ASTM size correction cannot effectively describe the effect of the significant constraint loss brought by mini-CT geometry. Despite the possible doubts regarding the validity of the ASTM size correction, it is important to note that the subsequent data censoring procedure employed in the evaluation of T_0 has been shown to be effective, although not perfect, for circumventing the effect of the significant loss of constraint and for compensating the limitation of the ASTM size correction. This can be seen in Fig. 11(b), where the $K_{Jclimit,mini\text{-}CT}$ defined with ASTM E1920 (the red box) falls close to the point where a significant loss of constraint is observed when using the local approach. In the red box, the 1T-normlizaed K_{Jc} of mini-CT using two different methods show close agreement. Proposing a size correction method based on the local approach offers a notable advantage when dealing with the K_{Jc} values that exceed the $K_{Jclimit}$. With this method, one can get rid of the data censoring procedure and allows for the evaluation of T_0 using only a limited number of data points.

Consequently, the size correction scheme is performed based on the $K_{Jc,mini\text{-}CT} \rightarrow$ 1T-nomalized $K_{Jc,mini\text{-}CT}$ correlation computed using the local approach with $m = 21$ and $\sigma_{prs} = 3800$ MPa. In order to keep the form consistent with the original ASTM size correction equation, when $K_{Jc,mini\text{-}CT} < 125$ MPa$\sqrt{}$m, a 5 MPa$\sqrt{}$m reduction can simply be applied to the ASTM size correction results. When $K_{Jc,mini\text{-}CT} \geq 125$ MPa$\sqrt{}$m, the power law part of the ASTM size correction equation should be adjusted. A new size correction scheme is proposed:

$$K_{Jc,1T} = \begin{cases} 20 + \left[K_{Jc,mini-CT} - 20\right]\left(\frac{B_{mini-CT}}{B_{1T}}\right)^{\frac{1}{4}} - 5 & for \quad K_{Jc,mini-CT} < 125MPa\sqrt{\text{m}} \\ 20 + \left[K_{Jc,mini-CT} - 20\right]\left(\frac{B_{mini-CT}}{B_{1T}}\right)^{\frac{1}{4}+\frac{K_{Jc,mini-CT}-125}{650}} - 5 & for \quad K_{Jc,mini-CT} \geq 125MPa\sqrt{\text{m}} \end{cases} \tag{11}$$

4.2. Application of the new size correction scheme to 22NiMoCr37

The above discussion clearly shows the capability of the local approach as employed here for correcting the fracture toughness value of the mini-CT geometry to its 1-inch size equivalence. As the new size correction scheme aims to correct all the experimental data obtained from mini-CT, the following sections will examine its practical application across various materials.

The new size correction scheme is first applied to the 22NiMoCr37 steel. According to the requirements in ASTM E1921, the test temperature should satisfy -50 °C ≤ T - T_0 ≤ 50 °C. For the mini-CT geometry, the tests must be performed in a lower temperature range to avoid too many data exceeding the maximum allowable toughness and being censored [4]. Therefore, mini-CT specimens in the present study were tested in the temperature range from -150 °C to -115 °C. The validity of the present size correction scheme is verified in this test temperature regime. Table 6 provides the Weibull fitting parameter, K_0, determined from the master curve of mini-CT with T_0 = -107 °C ($K_{0,mini-CT}$), and the 1T-normalized K_0 ($K_{0,1T-local}$) corrected from the $K_{0,mini-CT}$ based on the current procedure. To facilitate the comparison, Table 6 also includes the K_0 determined from the master curve with T_0 = -95 °C that is derived from large CTs ($K_{0,1T-CT}$). The agreement between $K_{0,1T-local}$ and $K_{0,1T-CT}$ is very good within the current test temperature range (-150 °C ~ -115 °C), showing a maximum difference of only 6.7 MPa$\sqrt{\text{m}}$. The present approach with m = 21, σ_{prs} = 3800 MPa provides accurate size correction of the fracture toughness of mini-CT in the test temperature range between -150 °C and -115 °C.

Now the correction capability of the present approach is accessed, by showing that the "true" reference temperature, T_0, can be determined based on the test data at all test temperatures. First, by applying the size correction scheme outlined in Eq. (10), the K_{Jc} values measured from the mini-CT specimens for T_{test} = -150 ~ -115 °C are corrected to their 1T size equivalence. T_0 is then computed based on the corrected 1T-normalized K_{Jc} data using the evaluation procedure given in ASTM E1921. The only difference made in the T_0 evaluation procedure in the present study is the size correction of the fracture toughness and whether or not the data needs to be censored according to $K_{Jclimit}$. As shown in Table 7, using the ASTM size correction methodology, twelve data are censored, whereas using the new size correction, this number is reduced by 50%. The T_0 value evaluated based on the local approach size correction is equal to -99.5 °C, which is 7.2 °C closer to the T_0 = -95 °C determined from large CT specimens when compared to the ASTM size correction. If no data censoring is applied, T_0 yields the value of -100.3 °C, which is still consistent. Therefore, the new size correction laws allow the generation of a reliable T_0 which is closer to that determined from standard large CT geometries without wasting a single test data.

Fig. 12 provides the master curve and associated lower and upper bounds when T_0 = -100.3 °C, and the K_{Jc} data corrected using the new size correction and the ASTM size correction. This master curve is expected to show a close K_{Jc} distribution to the master curve of large CT geometries owing to similar T_0 value. This is because the master curve solely relies on T_0, as demonstrated in Eq. (9). Although the size corrected K_{Jc} values that exceed the $K_{Jclimit}$ will not be used in the evaluation of the master curve, it is clear that, from the perspective of the performance of the size correction method, the K_{Jc} data corrected using the local approach has a more reasonable distribution around the 5% and 95% confidence bounds. By contrast, the ASTM size correction method exhibits a relatively poor performance at higher test temperature, with much larger corrected K_{Jc} value. Indeed, due to constraint loss, higher measured K_{Jc} is almost unavoidable in a mini-CT, whereas the size correction scheme based on the local approach can effectively reduce this effect.

4.3. Application of the new size correction scheme on other RPV steels

The same size correction equations are applied on the test data of two other RPV steels: un-irradiated 73W steel and irradiated A508 Cl.3 steel [8]. Before conducting the size correction, the identification procedure for the m factor and σ_{prs} is carried out for different materials: 22NiMoCr37 at RT, un-irradiated 73W at -100 °C and irradiated A508 Cl.3 at -75 °C, respectively. The purpose of repeating this calibration is to examine the correlation of $K_{Jc,mini-CT}$ and its 1T size equivalence determined by their corresponding calibrated local approaches for each of these materials, and to further establish the generality of the new size correction equations proposed

Table 6
Summary of the predicted K_0 at different temperature in the temperature range of interest.

T (°C)	Experimental results		Local approach predictions	($K_{0,1T-CT}$ - $K_{0,1T-local}$)/$K_{0,1T-CT}$
	$K_{0,mini-CT}$* (MPa$\sqrt{\text{m}}$)	$K_{0,1T-CT}$* (MPa$\sqrt{\text{m}}$)	$K_{0,1T-local}$ (MPa$\sqrt{\text{m}}$)	
-90	204.2	115.6	108.9	-5.8%
-115	151.4	88.8	92.6	4.3%
-130	115.4	70.5	75.6	7.2%
-150	90.7	58.0	59.9	3.3%

*: these are not derived from experimental data at the corresponding test temperature but estimated following their master curves.

Table 7
Summary of the T_0 determination using different size correction methods.

	Mini-CT			Standard large CT
	ASTM size correction	NEW size correction		
		With data censoring	Without data censoring	
N	51	51	51	–
r	39	45	51	–
Number of censored data N - r	12	6	0	–
T_0 (°C)	-106.7	-99.5	-100.3	-95

N = the total number of the test data, r = the number of the uncensored data.

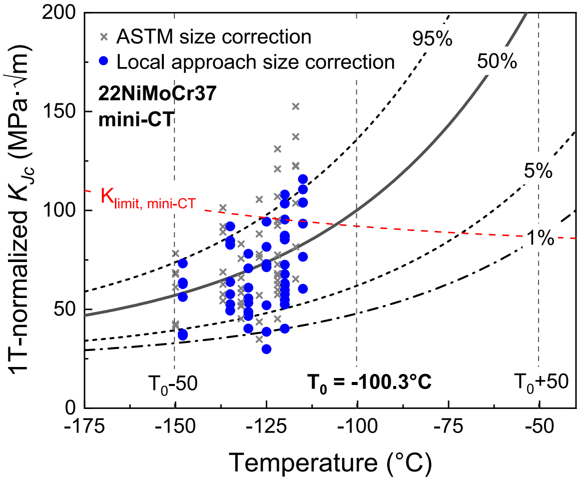

Fig. 12. Fracture toughness distribution and associated Master Curve of mini-CT geometry generated using the local approach.

above. The identified parameters are listed in Table 8. Please note that in this study, the definition of the m factor is based on an assumption within a reasonable range. Therefore, the m factor for all analyzed RPV steels is assumed to be a constant value of 21. With this constant m factor, the corresponding σ_{prs} can be identified for different material properties.

The correlation between the fracture toughness of the mini-CT geometry, $K_{Jc,mini\text{-}CT}$, and its 1T size equivalence is obtained based on the σ_w - K_{Jc} trajectories of 1T-CT geometry and mini-CT geometry obtained from the calibrated local approaches of different materials, the results are summarized in Fig. 13. It is worth noting that the correlation between $K_{Jc,mini\text{-}CT}$ and its 1T size equivalence is much more dependent on the specimen size than on material properties. In particular, the $K_{Jc,mini\text{-}CT}$ -1T normalized $K_{Jc,mini\text{-}CT}$ trajectories of different materials display remarkable agreement, with the maximum difference in the determined 1T normalized $K_{Jc,mini\text{-}CT}$ being approximately 7.5 MPa$\sqrt{\text{m}}$. This deviation is small, as a result, the size correction equations generated from these materials will be almost identical. Therefore, it is reasonable to apply the same size correction equations to the materials discussed in the subsequent sections. As mentioned earlier, any bias resulting from the selection of the m factor can be compensated to some extent by the value of σ_{prs}. Thus, it can be inferred that using a different value of m factor would not have a significant impact on the results.

As shown in Fig. 14, the corrected K_{Jc} data for both materials using the new size correction are within a more reasonable range characterized by the master curve identified on large geometries. Adequate T_0 results are obtained when data censoring is ignored in the context of the new size correction method (see Table 9). It is worth mentioning that, for the un-irradiated 73W steel, the deviation of T_0 for mini-CT and 1T-CT may be due to the inhomogeneity of the weld, because the location of the crack in the weld (fine grain and coarse grain) can have influence on the results. Moreover, the small sampling zone in front of the crack tip of mini-CT specimen makes it particularly sensitive to the effect of material inhomogeneity, which requires follow-up investigations.

Above all, for the mini-CT geometry, the reliable T_0 value provided by the current ASTM size correction method relies on a strict data censoring. As a result, all measured K_{Jc} values that exceed the $K_{Jclimit}$ will not be considered in the evaluation of T_0. However, the new micromechanics-based size correction method allows the replacement of the data censoring and thus the relaxation of the $K_{Jclimit}$, because it can provide stable T_0 value whether or not a data censoring is applied. Therefore, the significance of the new size correction method lies in approaching the T_0 to that determined based on standard large CT geometries, while ensuring the unique meaning of each single test data.

5. Summary and conclusions

Due to the significant loss of constraint, higher fracture toughness values tend to be generated from the mini-CT. Current size effect

Table 8
Summary of the m factor and σ_{prs} for different materials.

	m	σ_{prs} (MPa)
22NiMoCr37 (-110 °C)	21	3800
22NiMoCr37 (RT)	21	3900
73W (-100 °C)	21	4000
Irradiated A508 Cl.3 (-75 °C)	21	4100

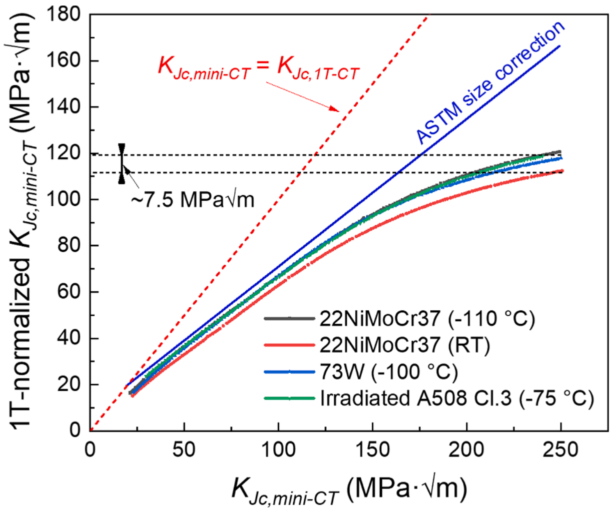

Fig. 13. Correlations of 1T-normalized K_{Jc} and the K_{Jc} measured from mini-CT specimen for different materials.

correction for the fracture toughness introduced in ASTM E1921 only takes into account the effect of thickness and is therefore inadequate for providing effective size correction for the measured K_{Jc} of mini-CT specimens in the test temperature close to the reference temperature, T_0. Although the $K_{Jclimit}$ censoring procedure ensures that reliable T_0 can be computed, it comes with a large number of test data being censored, leading to a significant loss of time, money and material, particularly in the irradiation-related investigations.

This study proposes a new size correction of the fracture toughness measured with mini-CT specimens in the ductile-to-brittle transition (DBT) region. The central feature of this size correction scheme lies in the interpretation of the local approach to brittle fracture coupled with finite element simulations. The size correction scheme starts with the calibration of the local approach, thereby establishing the connection between the geometries with different constraints. Based on the connections, the new size correction scheme is proposed, which allows direct conversion from the measured $K_{Jc,mini-CT}$ to its 1T size equivalence and, consequently, contributes to the evaluation of the transition temperature, T_0, and to the establishment of the Master Curve.

Application of the new size correction scheme based on the local approach provides reliable 1T-normalized K_{Jc} values, the distribution of the corrected data being in a more reasonable agreement with lower and upper bound curves derived from larger size specimens. Compared to the current method given in the ASTM standard, the new size correction reduces significantly the number of censored data by 50%, and brings the calculated T_0 value (T_0 = -99.5 °C) 7.2 °C closer to the calculated T_0 from large CT specimens (T_0 = -95 °C). In particular, the present size correction enables the replacement of the data censoring procedure and thus the relaxation of the $K_{Jclimit}$, which limit the waste of test data and can provide a close T_0 value (T_0 = -100.3 °C). Application of this new size correction method to two other RPV steels also demonstrated its remarkable ability to characterize the fracture toughness in the DBT region. It is worth noting that, the advantage of the current strategy of proposing a series of size correction equations is that it is only based on the experimental data of mini-CT geometry. This strategy, which does not rely on more test data from other geometries, provides a basis for further investigations and extensions to a wide range of alloys.

CRediT authorship contribution statement

Meng Li: Writing – review & editing, Writing – original draft, Visualization, Validation, Methodology, Investigation, Data curation, Conceptualization. **Rachid Chaouadi:** Writing – review & editing, Supervision, Software, Resources, Project administration, Data curation, Conceptualization. **Inge Uytdenhouwen:** Writing – review & editing, Supervision, Software, Resources, Project administration, Data curation. **Thomas Pardoen:** Writing – review & editing, Supervision, Resources.

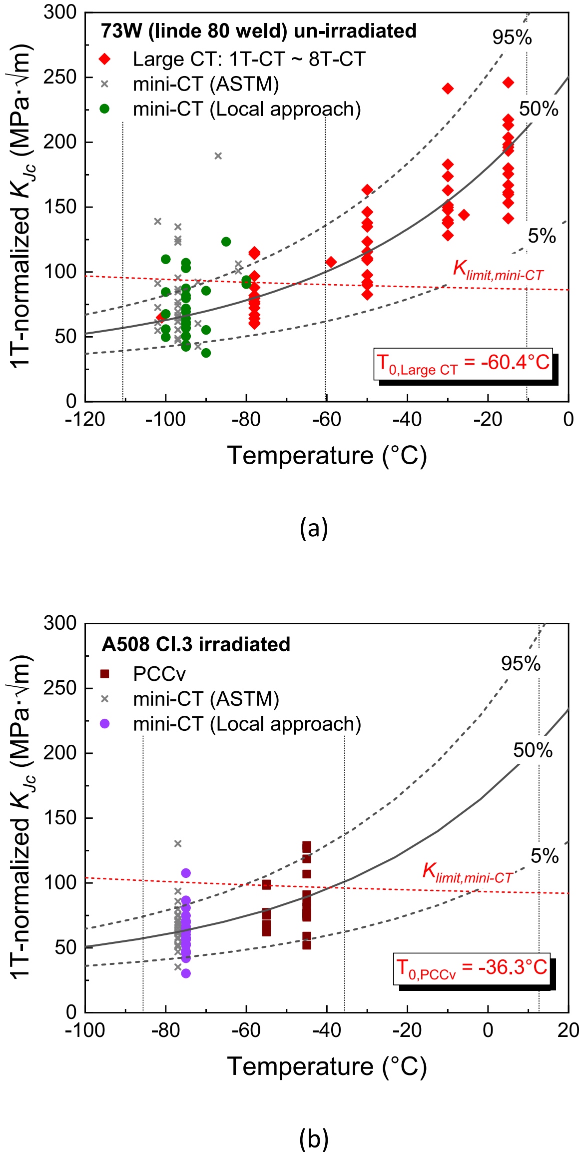

Fig. 14. Size correction on the fracture toughness of (a) un-irradiated 73W steel and (b) irradiated A508 Cl.3 steel.

Table 9
Summary of the T_0 determination using different size correction methods for un-irradiated 73W steel and irradiated A508 Cl.3 steel.

		Mini-CT				Large geometries
		ASTM size correction		NEW size correction		
		With data censoring	Without data censoring	With data censoring	Without data censoring	
73W un-irradiated	N - r	9	0	8	0	1
	T_0 (°C)	-76.0	-92.0	-72.7	-75.3	-60.4
A508 Cl.3 irradiated	N - r	1	0	1	0	0
	T_0 (°C)	-43.2	-49.8	-38.3	-39.2	-36.3*

N-r: Number of censored data. *: the T_0 of PCCv is slightly lower than that of standard large CT geometries.

Declaration of Competing Interest

The authors declare that they have no known competing financial interests or personal relationships that could have appeared to influence the work reported in this paper.

Data availability

Data will be made available on request.

Acknowledgements

The present work was performed within the SUSTAIN project at SCK CEN supported by the NMS management. In addition, part of the work was done under the FRACTESUS project that has received funding from the Euratom research and training program 2020-2024 under grant agreement No. 900014. The authors gratefully acknowledge the support of the technical staff of LHMA at SCK CEN. The authors also acknowledge SCK CEN Academy for PhD funding. Additionally, the authors would like to acknowledge the late Dr. Tomasz Brynk for his extensive contributions to this work.

References

[1] ASTM, ASTM E1921-19b, in Standard Test Method for Determination of Reference Temperature, T_0, for Ferritic Steels in the Transition Range. 2020, ASTM International: West Conshohocken, PA.
[2] Sokolov MA. Use of Mini-CT Specimens for Fracture Toughness Characterization of Low Upper-Shelf Linde 80 Weld Before and After Irradiation. Pressure Vessels and Piping Conference. American Society of Mechanical Engineers; 2018.
[3] Yamamoto M, et al. A round robin program of Master Curve evaluation using miniature C (T) specimens: First round robin test on uniform specimens of reactor pressure vessel material. Pressure Vessels and Piping Conference. American Society of Mechanical Engineers; 2012.
[4] Chaouadi, R., et al. *On the use of miniaturized CT specimens for fracture toughness characterization of RPV materials*. in *ASME 2016 Pressure Vessels and Piping Conference*. 2016. American Society of Mechanical Engineers, PVP2016-63607.
[5] Sánchez M, Cicero S, Kirk M, Altstadt E, Server W, Yamamoto M. Using Mini-CT Specimens for the Fracture Characterization of Ferritic Steels within the Ductile to Brittle Transition Range: A Review. Metals 2023;13(1):176.
[6] Lucon E, Scibetta M, Chaouadi R, van Walle E, Dean SW. Use of miniaturized compact tension specimens for fracture toughness measurements in the upper shelf regime. J ASTM Int 2006;3(1):13235.
[7] Scibetta, M., *Constraint assessment in miniature C (T) specimens using 3D finite element simulations*, in *SCK CEN Report BLG-923*. 2002.
[8] Lambrecht M, Chaouadi R, Li M, Uytdenhouwen I, Scibetta M. On the Possible Relaxation of the ASTM E1921 and ASTM E1820 Standard Specifications with Respect to the Use of the Mini-CT Specimen. Mater Perform Charact 2020;9(5):20190217.
[9] Pineau A, Benzerga AA, Pardoen T. Failure of metals I: Brittle and ductile fracture. Acta Mater 2016;107:424–83.
[10] Ruggieri C, Dodds Jr RH. An engineering methodology for constraint corrections of elastic–plastic fracture toughness–Part I: A review on probabilistic models and exploration of plastic strain effects. Engng Fract Mech 2015;134:368–90.
[11] Barbosa VS, Ruggieri C. A simplified estimation procedure for the Weibull stress parameter, m, and applications to predict the specimen geometry dependence of cleavage fracture toughness. Int J Press Vessel Pip 2020;188:104228.
[12] Brückner-Foit A, Ehl W, Munz D, Trolldenier B. The size effect of microstructural implications of the weakest link model. Fatigue Fract Eng Mater Struct 1990;13 (3):185–200.
[13] Epstein B. Statistical aspects of fracture problems. J Appl Phys 1948;19(2):140–7.
[14] Takamizawa H, et al. Finite Element Analysis on the Application of Mini-C (T) Test Specimens for Fracture Toughness Evaluation. Pressure Vessels and Piping Conference. American Society of Mechanical Engineers; 2015.
[15] Miura N, Soneda N. Evaluation of fracture toughness by master curve approach using miniature C (T) specimens. J Press Vessel Technol 2012;134(2).
[16] Tobita T, Nishiyama Y, Ohtsu T, Udagawa M, Katsuyama J, Onizawa K. Fracture toughness evaluation of reactor pressure vessel steels by master curve method using miniature compact tension specimens. J Press Vessel Technol 2015;137(5).
[17] Sugihara T, et al. Applicability of miniature C (T) specimen to fracture toughness evaluation for the irradiated Japanese reactor pressure vessel steel. Pressure Vessels and Piping Conference. American Society of Mechanical Engineers; 2017.
[18] Ha Y, Tobita T, Ohtsu T, Takamizawa H, Nishiyama Y. Applicability of miniature compact tension specimens for fracture toughness evaluation of highly neutron irradiated reactor pressure vessel steels. J Press Vessel Technol 2018;140(5).
[19] Chen X, et al. Specimen Size and Geometry Effects on the Master Curve Fracture Toughness Measurements of EUROFER97 and F82H Steels. Pressure Vessels and Piping Conference. American Society of Mechanical Engineers; 2022.
[20] Sokolov MA. Use of Mini-CT Specimens for Fracture Toughness Characterization of Irradiated Highly Embrittled Weld. Pressure Vessels and Piping Conference. American Society of Mechanical Engineers; 2022.
[21] Chaouadi, R., *Analysis of toughness behavior of 22NiMoCr37 steel in the transition regime (SM&T Round Robin)*, in *SCK CEN Report BLG-799*. 1998.
[22] Heerens J, Hellmann D. Development of the Euro fracture toughness dataset. Engng Fract Mech 2002;69(4):421–49.
[23] Heerens J, Hellmann D. *Fracture toughness of steel in the ductile to brittle transition regime*, in *Final Report of the EU-Project MAT-CT-940080*. Germany: GKSS-Research Center; 1999.
[24] Bridgman P. The stress distribution at the neck of a tension specimen. Trans. Amer Soc 1944.
[25] Anderson TL. Fracture mechanics: fundamentals and applications. CRC Press; 2017.
[26] Gao X, Ruggieri C, Dodds R. Calibration of Weibull stress parameters using fracture toughness data. Int J Fract 1998;92(2):175–200.
[27] Ruggieri C, Savioli RG, Dodds Jr RH. An engineering methodology for constraint corrections of elastic–plastic fracture toughness–Part II: Effects of specimen geometry and plastic strain on cleavage fracture predictions. Engng Fract Mech 2015;146:185–209.
[28] Pardoen T, Hutchinson J. Micromechanics-based model for trends in toughness of ductile metals. Acta Mater 2003;51(1):133–48.
[29] Petti JP, Dodds Jr RH. Calibration of the Weibull stress scale parameter, σu, using the Master Curve. Engng Fract Mech 2005;72(1):91–120.
[30] Beremin FM, Pineau A, Mudry F, Devaux J-C, D'Escatha Y, Ledermann P. A local criterion for cleavage fracture of a nuclear pressure vessel steel. Metall Trans A 1983;14(11):2277–87.
[31] Mudry F. A local approach to cleavage fracture. Nucl Engng Des 1987;105(1):65–76.
[32] Wallin K, Saario T, Törrönen K. Fracture of brittle particles in a ductile matrix. Int J Fract 1986;32(3):201–9.
[33] Ruggieri C. Influence of threshold parameters on cleavage fracture predictions using the Weibull stress model. Int J Fract 2001;110:281–304.
[34] Gao X, et al. A Weibull stress model to predict cleavage fracture in plates containing surface cracks. Fatigue Fract Eng Mater Struct 1999;22(6):481–93.
[35] Andrieu A, Pineau A, Besson J, Ryckelynck D, Bouaziz O. Beremin model: Methodology and application to the prediction of the Euro toughness data set. Engng Fract Mech 2012;95:102–17.
[36] Ruggieri C, Gao X, Dodds Jr RH. Transferability of elastic–plastic fracture toughness using the Weibull stress approach: significance of parameter calibration. Engng Fract Mech 2000;67(2):101–17.
[37] Wiesner, C. and M. Goldthorpe, *The effect of temperature and specimen geometry on the parameters of the" Local Approach" to cleavage fracture.* Le Journal de Physique IV, 1996. **6**(C6): p. C6-295-C6-304.
[38] Qian X, Chen S. A K0-based calibration procedure for the Weibull stress cleavage model. Fatigue Fract Eng Mater Struct 2014;37(4):391–405.

[39] Cao Y, Hui Hu, Wang G, Xuan F-Z. Inferring the temperature dependence of Beremin cleavage model parameters from the Master Curve. Nucl Engng Des 2011; 241(1):39–45.

[40] Bhattacharyya K, Acharyya S, Dhar S, Chattopadhyay J. Calibration of Beremin parameters for 20MnMoNi55 steel and prediction of reference temperature (T 0) for different thicknesses and a/W ratios. J Fail Anal Prev 2018;18(6):1534–47.

[41] Coppejans, O. and C. Walters. *Comparison of methods to find the Weibull stress parameters*. in *International Conference on Offshore Mechanics and Arctic Engineering*. 2018. American Society of Mechanical Engineers.

[42] Wasiluk B, Petti JP, Dodds Jr RH. Temperature dependence of Weibull stress parameters: Studies using the Euro-material. Engng Fract Mech 2006;73(8): 1046–69.

[43] Ruggieri C, Dodds Jr R, Wallin K. Constraint effects on reference temperature, T0, for ferritic steels in the transition region. Engng Fract Mech 1998;60(1): 19–36.

[44] Ruggieri C, Dodds RH. A transferability model for brittle fracture including constraint and ductile tearing effects: a probabilistic approach. Int J Fract 1996;79 (4):309–40.